Gauge dependence of calculations in relativistic Coulomb excitation

B. F. Bayman
School of Physics and Astronomy, University of Minnesota, 116 Church Street S.E., Minneapolis, Minnesota 55455

F. Zardi
Istituto Nazionale di Fisica Nucleare and Dipartimento di Fisica, Via Marzolo, 8, I-35131 Padova, Italy

(Received 27 October 2004; published 27 January 2005)

Before a quantum-mechanical calculation involving electromagnetic interactions is performed, the gauge to be used in expressing the potentials must be chosen. If the calculation is done exactly, the observable results it predicts will be independent of the choice of gauge. However, in most practical calculations, approximations are made, which can destroy the gauge invariance of the predictions. We compare here the results of coupled-channel time-dependent relativistic Coulomb excitation calculations as performed in either Lorentz or Coulomb gauges. We find significant differences when the bombarding energy per nucleon is $\geqslant 2$ GeV, which indicates that the common practice of relying completely on the Lorentz gauge can be dangerous.

DOI: 10.1103/PhysRevC.71.014904 PACS number(s): 25.70.De, 25.75.−q, 24.30.Cz

I. INTRODUCTION

Coulomb excitation is a collison process in which the predominant projectile-target interaction is electromagnetic. The electromagnetic interaction is expressed in the Hamiltonian, and therefore also in the Schrödinger equation, in terms of the electromagnetic potentials, $(\varphi(\mathbf{r}, t), \mathbf{A}(\mathbf{r}, t))$. The potentials are subject to gauge ambiguity, since they are not uniquely determined by the charge and current distributions that create the electromagnetic field. Equivalently, if a gauge transformation generated by $\Lambda(\mathbf{r}, t)$ is performed, the new potentials $(\varphi'(\mathbf{r}, t), \mathbf{A}'(\mathbf{r}, t))$ defined by

$$\varphi'(\mathbf{r}, t) \equiv \varphi(\mathbf{r}, t) - \frac{1}{c}\frac{\partial \Lambda(\mathbf{r}, t)}{\partial t} \tag{1.1a}$$

$$\mathbf{A}'(\mathbf{r}, \mathbf{t}) \equiv \mathbf{A}(\mathbf{r}, t) + \nabla \Lambda(\mathbf{r}, t) \tag{1.1b}$$

yield the same $(\mathbf{E}(\mathbf{r}, t), \mathbf{B}(\mathbf{r}, t))$ as did $(\varphi(\mathbf{r}, t), \mathbf{A}(\mathbf{r}, t))$ [1]. Thus $(\varphi(\mathbf{r}, t), \mathbf{A}(\mathbf{r}, t))$ and $(\varphi'(\mathbf{r}, t), \mathbf{A}'(\mathbf{r}, t))$ are both consistent with Maxwell's equations and the given charge and current distributions. Since the Schrödinger equation depends explicitly on the potentials, it is changed by a gauge transformation, and so is the wave function that is the solution of the Schrödinger equation. However, when an observable quantity (such as a transition probability) is calculated from this wave function, the result is invariant under a gauge transformation, even though the wave function is not.

The gauge invariance of an observable applies only if the exact solution of the Schrödinger equation is used in its calculation. If an approximate solution is used, then the calculated observable quantity may or may not be gauge invariant. A non-gauge invariant prediction is a serious drawback for a theory, since there is generally no *a priori* reason to choose one gauge rather than another.

An example of an approximate solution that *is* gauge invariant is given by first-order time-dependent perturbation theory [2]. Suppose we want to estimate transition probabilities in the target under the influence of a time-dependent external potential $V(\mathbf{r}, t)$ provided by the projectile. If we use first-order time-dependent perturbation theory, then the predicted transition probability from target state ϕ_α at $t = -\infty$ to target state ϕ_γ at $t = \infty$ is given by

$$\left| \int_{-\infty}^{\infty} \frac{dt}{i\hbar} e^{i\omega_{\gamma\alpha} t} V_{\gamma\alpha}(t) \right|^2,$$

where

$$\omega_{\gamma\alpha} \equiv (\epsilon_\gamma - \epsilon_\alpha)/\hbar \tag{1.2a}$$

$$V_{\gamma\alpha}(t) \equiv \langle \phi_\gamma | V(\mathbf{r}, t) | \phi_\alpha \rangle. \tag{1.2b}$$

Thus the first-order transition probability is proportional to the square of the modulus of the $\omega = \omega_{\gamma\alpha}$ (onshell) Fourier component of $V_{\gamma\alpha}(t)$. If $\rho_{\gamma\alpha}$ and $\mathbf{J}_{\gamma\alpha}(\mathbf{r}, t)$ are the target transition charge and current densities associated with the $\phi_\alpha \rightarrow \phi_\gamma$ transition, the electromagnetic interaction $V_{\gamma\alpha}(t)$ is

$$V_{\gamma\alpha}(t) = \int d^3r \left[\rho_{\gamma\alpha}(\mathbf{r})\varphi(\mathbf{r}, t) - \frac{1}{c}\mathbf{J}_{\gamma\alpha}(\mathbf{r}) \cdot \mathbf{A}(\mathbf{r}, t) \right]. \tag{1.3}$$

Target charge conservation can be expressed by the relation

$$\nabla \cdot \mathbf{J}_{\gamma\alpha}(\mathbf{r}, t) + i\omega_{\gamma\alpha}\rho_{\gamma\alpha}(\mathbf{r}) = 0. \tag{1.4}$$

This can be used to show that the ω Fourier component of $V_{\gamma\alpha}(t)$,

$$V_{\gamma\alpha}(\omega) \equiv \int_{-\infty}^{\infty} \frac{dt}{i\hbar} e^{i\omega t} V_{\gamma\alpha}(t) \tag{1.5a}$$

$$= \int_{-\infty}^{\infty} \frac{dt}{i\hbar} e^{i\omega t} \int d^3r \times \left[\rho_{\gamma\alpha}(\mathbf{r})\varphi(\mathbf{r}, t) - \frac{1}{c}\mathbf{J}_{\gamma\alpha}(\mathbf{r}, t) \cdot \mathbf{A}(\mathbf{r}, t) \right], \tag{1.5b}$$

is changed by the gauge transformation[1] generated by $\Lambda(\mathbf{r}, t)$ by

$$\frac{(\omega - \omega_{\gamma\alpha})}{\hbar c} \int_{-\infty}^{\infty} dt \int d^3r e^{i\omega t} \rho_{\gamma\alpha}(\mathbf{r}) \Lambda(\mathbf{r}, t).$$

Thus the onshell, $\omega = \omega_{\gamma\alpha}$, Fourier component $V_{\gamma\alpha}(\omega_{\gamma\alpha})$, which determines the first-order transition probability, is unchanged by a gauge transformation.

There are other approximations that depend only on the onshell Fourier transform of the interaction. For example, in the model in which the target is represented by a harmonic oscillator and the interaction is assumed to be linear in the oscillating variable or its conjugate momentum, an exact solution of the time-dependent Schrödinger equation is available [3]. It depends only on the onshell Fourier transform of the time-dependence of the interaction. Also, the Fermi-Weizsacker-Williams (FWW) "method of virtual quanta" (see, e.g., Ref. [4]) is essentially first-order perturbation theory, in which the perturbing electromagnetic field is approximated by a plane wave. For both theories, the gauge independence of the onshell Fourier transform of the interaction guarantees that their predictions are gauge invariant.

However, this gauge invariance is not guaranteed if the full electromagnetic interaction is used, or if one wishes to go beyond first-order perturbation theory. For example, a coupled-channel approach to the time-dependent Schrödinger equation has been used in an attempt to get a better description of Coulomb excitation to multiphonon states of giant resonances [4–11]. One begins by choosing a set of target states that can be expected to play a significant role in the reaction and then solving the Schrödinger equation within the Hilbert space defined by these states. This coupled-channel approach depends upon the entire ω-dependence of $V_{\gamma\alpha}(\omega)$, not only on its value for $\omega = \omega_{\gamma\alpha}$. If all the target states were included in the calculation, then the coupled-channel solution of the Schrödinger equation would be exact, and calculated observables would be gauge invariant. However, if, as is always the case, the set of target states is truncated to make the calculation feasible, then the result of the coupled-channel calculation is approximate, and therefore calculated observables are not gauge invariant. The main concern of this paper is the lack of gauge invariance of the predictions of coupled-channel time-dependent solutions of the Schrödinger equation governing relativistic Coulomb excitation. Some related discussions of this subject have been given by Baltz, Rhoades-Brown, and Weneser [12], Rumrich and Greiner [13], and Kobe and Kennedy [14].

The classic paper on relativistic Coulomb excitation [2] by A. Winther and K. Alder (WA) described the electromagnetic influence of the projectile on the target using classical electromagnetic fields in the Lorentz gauge. Because the main concern of WA was first-order time-dependent perturbation theory, their calculated transition probabilities and cross sections were gauge invariant. Subsequent workers in this field who used coupled-channel methods continued to use classical fields and the Lorentz gauge. However, as explained above, the extent to which the results of these calculations are gauge invariant is not certain.

When studies are done in which the electromagnetic field is quantized, it is common to use the Coulomb (or transverse) gauge. The reason is that the field quanta (photons) will then be purely transverse. Table I compares the properties of the potentials in the Lorentz and Coulomb gauges.

We consider two models for the radial density of the projectile, as seen in its own rest frame: a finite spherically symmetric charge distribution, and a point charge. The expressions for the finite charge distribution are presented as Fourier transforms, which are convenient for the multipole expansions needed when the initial and final nuclear states are angular momentum eigenstates. The point charge expressions are presented as functions of t, which can be easily interpreted. Numerical calculations show that there is very little difference between the predictions of the two models.

In Section II we find the generator $\Lambda(\mathbf{r}, t)$, which will take us from the commonly used Lorentz gauge to the Coulomb gauge in the classical-field approach to relativistic Coulomb excitation. This generator is already known for a point projectile [12], but we derive the expression appropriate to a projectile of finite size. Section III presents the interaction potentials calculated in these two gauges. In Sec. IV we compare multipole expansions of these potentials and show that the Coulomb gauge potential is free of a divergence that appears in the Lorentz gauge potential at high bombarding energy. Sections V and VI apply these formulas to the excitation of multiphonon states of the giant dipole resonance in ^{40}Ca, as a result of bombardment by ^{208}Pb nuclei. Section VII presents our conclusions and some general observations about gauge invariance.

II. THE GAUGE TRANSFORMATION CONNECTING THE LORENTZ AND COULOMB GAUGES

We follow the standard approach to relativisitic Coulomb excitation as proposed by WA. The projectile nucleus is assumed to travel along a straight-line orbit parallel to the $\hat{\mathbf{z}}$ axis, with impact parameter $\mathbf{b}$, at constant speed v. The magnitude of the impact parameter is large enough so that nuclear interactions between the target and projectile are negligible. Because of the assumed large projectile momentum, the electromagnetic impulse the projectile receives due to its interaction with the target has little effect on its trajectory, so the projectile maintains its constant speed and impact parameter throughout the collision. As the projectile passes, the target nucleus feels the time-dependent projectile electromagnetic fields, which induce transitions between the quantum states of the target.

We seek the gauge function $\Lambda(\mathbf{r}, t)$ that generates the gauge transformation

$$\mathbf{A}^C(\mathbf{r}, t) = \mathbf{A}^L(\mathbf{r}, t) + \nabla\Lambda(\mathbf{r}, t) \tag{2.1a}$$

$$\varphi^C(\mathbf{r}, t) = \varphi^L(\mathbf{r}, t) - \frac{1}{c}\frac{\partial}{\partial t}\Lambda(\mathbf{r}, t) \tag{2.1b}$$

between the potentials satisfying the Lorentz and Coulomb conditions listed in Table I.

[1] We restrict our attention to gauge generators that vanish at $t = \pm\infty$.

TABLE I. Comparison of the corresponding properties of the potentials in the Lorentz and Coulomb gauges, due to the projectile charge density $\rho_P(\mathbf{r}, t)$ and the current density $\mathbf{J}_P(\mathbf{r}, t)$.

Lorentz gauge	Coulomb gauge
$\nabla\cdot\mathbf{A}^L + \frac{1}{c}\frac{\partial}{\partial t}\varphi^L = 0$	$\nabla\cdot\mathbf{A}^C = 0$
$\nabla^2\varphi^L - \frac{1}{c^2}\frac{\partial^2}{\partial t^2}\varphi^L = -4\pi\rho_P$	$\nabla^2\varphi^C = -4\pi\rho_P$
$\nabla^2\mathbf{A}^L - \frac{1}{c^2}\frac{\partial^2\mathbf{A}^L}{\partial t^2} = -\frac{4\pi}{c}\mathbf{J}_P$	$\nabla^2\mathbf{A}^C - \frac{1}{c^2}\frac{\partial^2\mathbf{A}^C}{\partial t^2} - \frac{1}{c}\frac{\partial}{\partial t}\nabla\varphi^C = -\frac{4\pi}{c}\mathbf{J}_P$

A. Point projectile of charge $Z_P e$

For a point projectile of charge $Z_P e$, we have a charge density given by

$$\rho_P(\mathbf{r}, t) = Z_P e\delta(\mathbf{r} - \mathbf{b} - \hat{\mathbf{z}}vt) = Z_P e\delta\left(\boldsymbol{\rho} - \mathbf{b} + \hat{\mathbf{z}}(z - vt)\right). \tag{2.2}$$

If this charge density is used on the right-hand sides of the equations for φ in the second row of Table I, we get the solutions

$$\varphi^L(\mathbf{r}, t) = \frac{Z_P e}{\sqrt{\frac{(\boldsymbol{\rho}-\mathbf{b})^2}{\gamma^2} + (z - vt)^2}} \tag{2.3a}$$

$$\varphi^C(\mathbf{r}, t) = \frac{Z_P e}{\sqrt{(\boldsymbol{\rho} - \mathbf{b})^2 + (z - vt)^2}.} \tag{2.3b}$$

Baltz, Rhoades-Brown, and Weneser [12] used these potentials and Eq. (2.1b) to obtain

$$\begin{aligned}\Lambda(\mathbf{r}, t) &= c\int_{-\infty}^{t}[\varphi^L(\mathbf{r}, t') - \varphi^C(\mathbf{r}, t')]dt' \\ &= Z_P ec\int_{-\infty}^{t}\left[\frac{1}{\sqrt{\frac{(\boldsymbol{\rho}-\mathbf{b})^2}{\gamma^2} + (z - vt')^2}} - \frac{1}{\sqrt{(\boldsymbol{\rho} - \mathbf{b})^2 + (z - vt')^2}}\right]dt' \\ &= Z_P e\frac{c}{v}\log\left[\frac{(vt - z) + \sqrt{\frac{(\boldsymbol{\rho}-\mathbf{b})^2}{\gamma^2} + (z - vt)^2}}{(vt - z) + \sqrt{(\boldsymbol{\rho} - \mathbf{b})^2 + (z - vt)^2}}\right].\end{aligned} \tag{2.4}$$

Using this $\Lambda(\mathbf{r}, t)$ and Eq. (2.1a), we can calculate the vector potential in the Coulomb gauge. In contrast to the Lorentz gauge vector potential, it has a component perpendicular to the $\hat{\mathbf{z}}$ direction,

$$(\mathbf{A}^C)_z = Z_P e\frac{c}{v}\left[\frac{1}{\sqrt{(\boldsymbol{\rho} - \mathbf{b})^2 + (vt - z)^2}} - \frac{1}{\gamma\sqrt{(\boldsymbol{\rho} - \mathbf{b})^2 + \gamma^2(vt - z)^2}}\right] \tag{2.5a}$$

$$\begin{aligned}(\mathbf{A}^C)_\perp = Z_P e\frac{c}{v}(\boldsymbol{\rho} - \mathbf{b})\Bigg[&\frac{1}{\sqrt{(\boldsymbol{\rho} - \mathbf{b})^2 + \gamma^2(vt - z)^2}\left(\gamma(vt - z) + \sqrt{(\boldsymbol{\rho} - \mathbf{b})^2 + \gamma^2(vt - z)^2}\right)} \\ &- \frac{1}{\sqrt{(\boldsymbol{\rho} - \mathbf{b})^2 + (vt - z)^2}\left((vt - z) + \sqrt{(\boldsymbol{\rho} - \mathbf{b})^2 + (vt - z)^2}\right)}\Bigg],\end{aligned} \tag{2.5b}$$

while

$$(\mathbf{A}^L)_z = \frac{v}{c}\varphi^L(x, y, z, t) = Z_P e\frac{v}{c}\frac{\gamma}{\sqrt{(\boldsymbol{\rho} - \mathbf{b})^2 + \gamma^2(vt - z)^2}} \tag{2.5c}$$

$$(\mathbf{A}^L)_\perp = 0. \tag{2.5d}$$

It can be verified by direct calculation that this $\mathbf{A}^C(\mathbf{r}, t)$ is solenoidal, with $\nabla\cdot\mathbf{A}^C(\mathbf{r}, t) = 0$, as specified in Table I for the Coulomb gauge.

The presence of γ in the Lorentz gauge scalar and vector potentials [Eqs. (2.3a) and (2.5c)] has the effect of decreasing the effective duration of the time-dependent impulse experienced

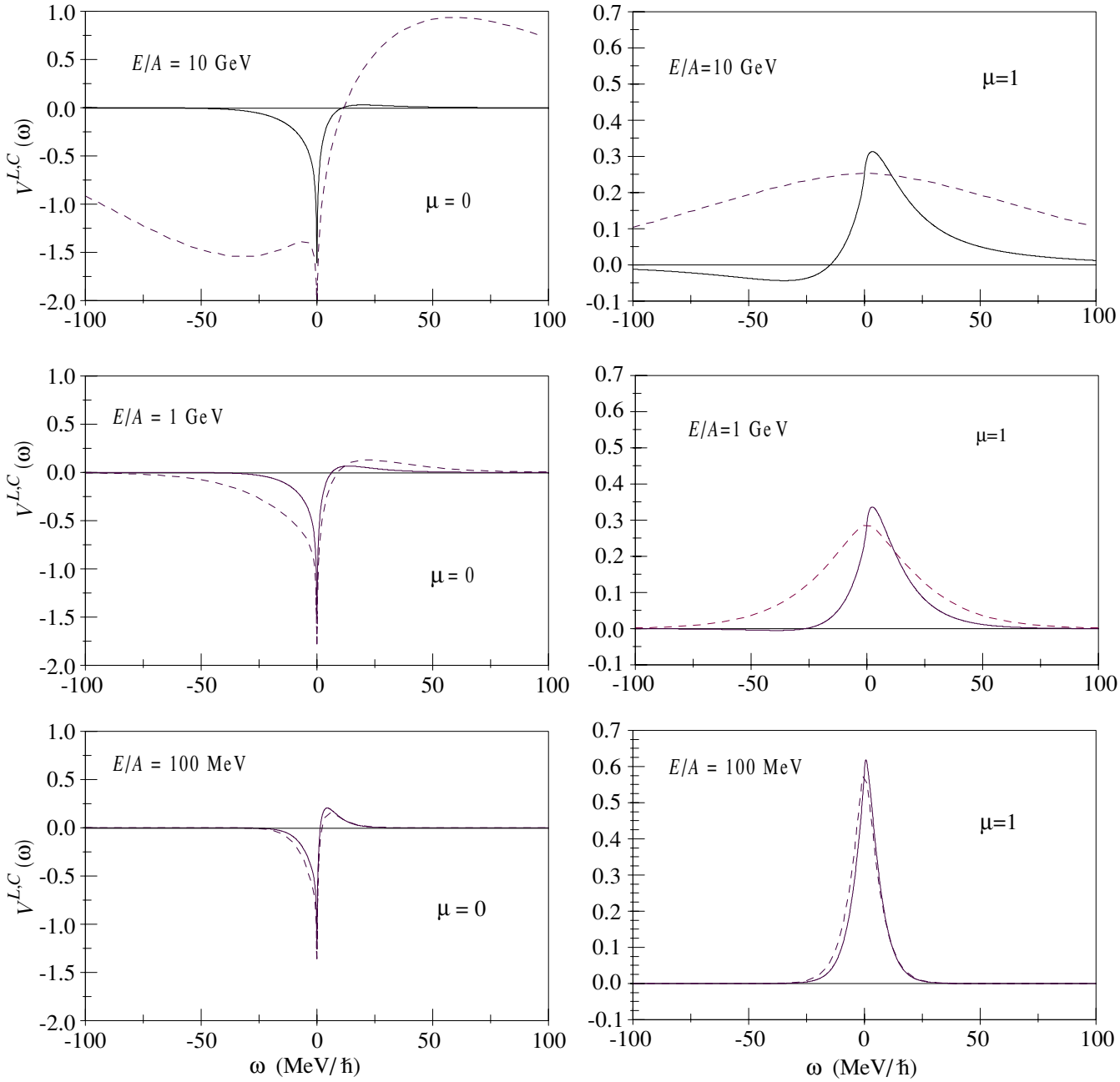

FIG. 1. Plots of matrix elements of $V^C(\omega)$ (solid lines) and $V^L(\omega)$ (dashed lines) connecting the ^{40}Ca ground state to the one-phonon giant dipole resonance states. The projectile is a ^{208}Pb nucleus with bombarding energies per nucleon specified within the figure frames. $\mu = 0$ corresponds to the $M = 0$ one-phonon state; $\mu = 1$ corresponds to the reflection-symmetric $|M| = 1$ state.

by the target. Note that the Coulomb gauge potentials [Eqs. (2.3b), (2.5a), and (2.5b)] have terms that are independent of γ. As a result, the Coulomb gauge pulse occurs over a longer time interval than does the Lorentz gauge pulse, and so the Coulomb gauge pulse is more adiabatic. This is illustrated in Figs. 1 and 2.

B. Finite spherically symmetric projectile of charge $Z_P e$

The method used in Section II A does not work for a finite-sized projectile. Whereas $\varphi^L(\mathbf{r}, t)$ is still given by Eq. (2.3a) (outside the projectile), the expression for $\varphi^C(\mathbf{r}, t)$ is more complicated than Eq. (2.3b). This is because the projectile, which is spherical in its own rest frame, appears flattened to an observer at the target, and Eq. (2.3b) is not a solution of Poisson's equation (second row and second column of Table I) for a flattened charge distribution.

The conditions in the first column of Table I are Lorentz covariant. Thus if $(\varphi^L, \mathbf{A}^L)$ satisfy the Lorentz gauge conditions in one Lorentz frame and they are subjected to a Lorentz transformation, then the transformed potentials will still satisfy

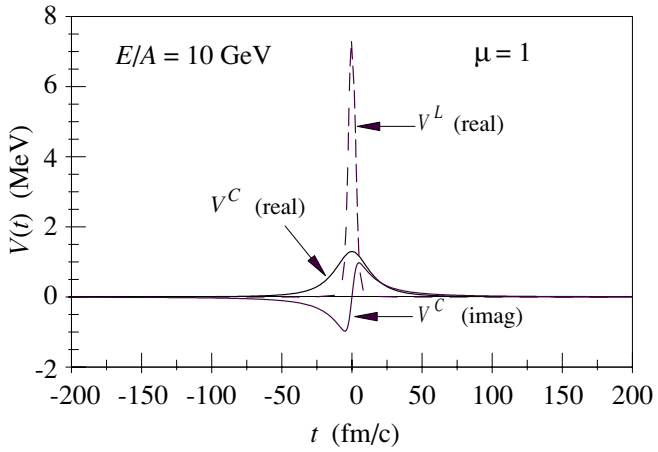

FIG. 2. Comparison of $V^C(t)$ (solid line) and $V^L(t)$ (dashed line), corresponding to the $E/A = 10$ GeV, $\mu = 1$ example of Fig. 1.

the Lorentz gauge conditions. This is *not* true for potentials satisfying the Coulomb gauge conditions given in the second column of Table I. If these potentials are subjected to a Lorentz transformation, the transformed potentials will generally *not* satisfy the Coulomb gauge conditions. In the calculation that follows, we begin with a static projectile charge distribution, viewed in the projectile rest frame. In this case, the ordinary Coulomb potential satisfies both the Lorentz and Coulomb gauge conditions. However, when we transform this potential to the target rest frame, the resulting potentials satisfy only the Lorentz conditions. If we want projectile potentials that satisfy the Coulomb conditions in the target frame, we must find a gauge transformation to take us to the Coulomb gauge from the potentials that have been obtained by Lorentz transformation from the projectile frame.

A necessary and sufficient condition for Eqs. (2.1a) and (2.1b) and Table I to be compatible is

$$\nabla^2\Lambda(\mathbf{r},t) = \frac{1}{c}\frac{\partial}{\partial t}\varphi^L(\mathbf{r},t). \tag{2.6}$$

To find a convenient expression for the right-hand side of Eq. (2.6), we start in the rest frame of the spherically symmetric projectile. Let $\tilde{x}$, $\tilde{y}$, $\tilde{z}(=\tilde{\mathbf{r}})$ be position coordinates measured relative to the projectile center-of-mass. Then the scalar potential $\tilde{\varphi}(\tilde{\mathbf{r}})$ satisfies

$$\nabla^2\tilde{\varphi}(\tilde{\mathbf{r}}) = -4\pi\rho_P(\tilde{\mathbf{r}}),$$

whose solution can be expressed[2] as

$$\begin{aligned}\tilde{\varphi}(\tilde{\mathbf{r}}) &= \frac{1}{2\pi^2}\int d^3r'\int d^3q\,\frac{e^{i\mathbf{q}\cdot(\tilde{\mathbf{r}}-\mathbf{r}')}}{q^2}\rho_P(\mathbf{r}')\\ &= \frac{2}{\pi}\int d^3q\,\frac{e^{i\mathbf{q}\cdot\tilde{\mathbf{r}}}}{q^2}\int_0^{R_P} r'^2dr'\,j_0(qr')\rho_P(r').\end{aligned} \tag{2.7}$$

It is assumed that all the projectile charge is contained within a sphere of radius R_P. The corresponding vector potential $\tilde{\mathbf{A}}(\tilde{\mathbf{r}})$ is zero.

[2]To ensure convergence, it may be necessary to replace $1/q^2$ by $\lim_{\eta\to 0}(1/(q^2+\eta^2))$.

If the projectile moves so that its center is located relative to the target by

$$\mathbf{r} = b\hat{\mathbf{y}} + vt\hat{\mathbf{z}} = \boldsymbol{\rho} + vt\hat{\mathbf{z}},$$

an observer at the target center will measure the scalar potential $\varphi_L(\mathbf{r},t)$ to be

$$\varphi_L(x,y,z,t) = \gamma\tilde{\varphi}(\tilde{x},\tilde{y},\tilde{z}) \tag{2.8}$$

with

$$\tilde{x} = x \tag{2.9a}$$

$$\tilde{y} = y - b \tag{2.9b}$$

$$\tilde{z} = \gamma(z - vt) \tag{2.9c}$$

$$\gamma = \left(1 - \frac{v^2}{c^2}\right)^{-1/2}. \tag{2.9d}$$

Thus we can write

$$\begin{aligned}\varphi^L(x,y,z,t) &= \frac{2\gamma}{\pi}\int d^3q\,\frac{e^{i\mathbf{q}\cdot(x\hat{\mathbf{x}}+(y-b)\hat{\mathbf{y}}+\gamma(z-vt)\hat{\mathbf{z}})}}{q^2}\\ &\quad\times\int_0^{R_P} r'^2dr'\,j_0(qr')\rho_P(r')\\ &= \frac{2\gamma}{\pi}\int_{-\infty}^{\infty}dq_z e^{iq_z\gamma(z-vt)}\int d^2q_\perp\frac{e^{i\mathbf{q}_\perp\cdot(\boldsymbol{\rho}-\mathbf{b})}}{q_\perp^2+q_z^2}\\ &\quad\times\int_0^{R_P} r'^2dr'\,j_0(qr')\rho_P(r')\\ &= \frac{2}{\pi}\int_{-\infty}^{\infty}dq_z e^{iq_z(z-vt)}\int d^2q_\perp\frac{e^{i\mathbf{q}_\perp\cdot(\boldsymbol{\rho}-\mathbf{b})}}{q_\perp^2+\left(\frac{q_z}{\gamma}\right)^2}\\ &\quad\times\int_0^{R_P} r'^2dr'\,j_0\left(\sqrt{q_\perp^2+\left(\frac{q_z}{\gamma}\right)^2}\,r'\right)\rho_P(r').\end{aligned} \tag{2.10}$$

If Eq. (2.10) is used in Eq. (2.6), we get

$$\begin{aligned}\nabla^2\Lambda(\mathbf{r},t) &= -\frac{2iv}{\pi c}\int dq_z q_z e^{iq_z(z-vt)}\int d^2q_\perp\frac{e^{i\mathbf{q}_\perp\cdot(\boldsymbol{\rho}-\mathbf{b})}}{q_\perp^2+\left(\frac{q_z}{\gamma}\right)^2}\\ &\quad\times\int_0^{R_p} r'^2dr'\,j_0\left(\sqrt{q_\perp^2+\left(\frac{q_z}{\gamma}\right)^2}\,r'\right)\rho_P(r'),\end{aligned}$$

whose solution can be written

$$\begin{aligned}\Lambda(\mathbf{r},t) &= \frac{2iv}{\pi c}\int_{-\infty}^{\infty}dq_z q_z e^{iq_z(z-vt)}\int d^2q_\perp\frac{e^{i\mathbf{q}_\perp\cdot(\boldsymbol{\rho}-\mathbf{b})}}{q^2\left(q_\perp^2+\left(\frac{q_z}{\gamma}\right)^2\right)}\\ &\quad\times\int_0^{R_p} r'^2dr'\,j_0\left(\sqrt{q_\perp^2+\left(\frac{q_z}{\gamma}\right)^2}\,r'\right)\rho_P(r')\\ &= \frac{2i}{\pi vc}\int_{-\infty}^{\infty}d\omega e^{-i\omega t}\omega e^{i\frac{\omega}{v}z}\end{aligned}$$

$$\times \int d^2q_\perp \frac{e^{i\mathbf{q}_\perp\cdot(\boldsymbol{\rho}-\mathbf{b})}}{\left(q_\perp^2+\left(\frac{\omega}{v}\right)^2\right)\left(q_\perp^2+\left(\frac{\omega}{\gamma v}\right)^2\right)} \times \int_0^{R_p} r'^2 dr' j_0\left(\sqrt{q_\perp^2+\left(\frac{\omega}{\gamma v}\right)^2}\, r'\right)\rho_P(r'), \tag{2.11}$$

in which we have replaced the integration variable q_z by $\omega \equiv q_z v$.

We can perform the $d^2q_\perp$ integration in (2.11) by using the relations

$$\frac{1}{q_\perp^2+\left(\frac{\omega}{v}\right)^2}\cdot\frac{1}{q_\perp^2+\left(\frac{\omega}{\gamma v}\right)^2}=\frac{c^2}{\omega^2}\left[\frac{1}{q_\perp^2+\left(\frac{\omega}{\gamma v}\right)^2}-\frac{1}{q_\perp^2+\left(\frac{\omega}{v}\right)^2}\right], \tag{2.12a}$$

$$\int d^2q_\perp \frac{e^{i\mathbf{q}_\perp\cdot(\boldsymbol{\rho}-\mathbf{b})}}{q_\perp^2+\left(\frac{\omega}{\gamma v}\right)^2} j_0\left(\sqrt{q_\perp^2+\left(\frac{\omega}{\gamma v}\right)^2}\, r'\right) = 2\pi K_0\left(\frac{|\omega||\boldsymbol{\rho}-\mathbf{b}|}{\gamma v}\right), \tag{2.12b}$$

$$\int d^2q_\perp \frac{e^{i\mathbf{q}_\perp\cdot(\boldsymbol{\rho}-\mathbf{b})}}{q_\perp^2+\left(\frac{\omega}{v}\right)^2} j_0\left(\sqrt{q_\perp^2+\left(\frac{\omega}{\gamma v}\right)^2}\, r'\right) = 2\pi K_0\left(\frac{|\omega||\boldsymbol{\rho}-\mathbf{b}|}{v}\right) j_0\left(i\frac{|\omega|}{c}r'\right). \tag{2.12c}$$

Equations (2.12b) and (2.12c), which are proven in the Appendix, are valid when $r' < |\boldsymbol{\rho}-\mathbf{b}|$. This condition is satisfied because of our assumption that b is large enough so that the projectile and target never overlap. Substituting Eqs. (2.12a)–(2.12c) into Eq. (2.11) leads to

$$\Lambda(\mathbf{r},t) = 4i\frac{c}{v}\int_{-\infty}^{\infty}\frac{d\omega}{\omega}e^{-i\omega t}e^{i\frac{\omega}{v}z}\left[\frac{Z_P e}{4\pi}K_0\left(\frac{|\omega||\boldsymbol{\rho}-\mathbf{b}|}{\gamma v}\right) - K_0\left(\frac{|\omega||\boldsymbol{\rho}-\mathbf{b}|}{v}\right)\int_0^{R_p} r'^2 dr' j_0\left(i\frac{|\omega|}{c}r'\right)\rho_P(r')\right].$$

This $\Lambda(\mathbf{r},t)$ will generate the transformation (2.1a,b) between the Lorentz and the Coulomb gauges.

III. INTERACTION MATRIX ELEMENTS

The matrix elements of the projectile-charge interaction in the two gauges are given by

$$[V^L(t)]_{\gamma\alpha} = \int d^3r\left[[\rho_T(\mathbf{r})]_{\gamma\alpha}\varphi^L(\mathbf{r},t) - \frac{1}{c}[\mathbf{J}_T(\mathbf{r})]_{\gamma\alpha}\cdot\mathbf{A}^L(\mathbf{r},t)\right] \tag{3.1a}$$

$$[V^C(t)]_{\gamma\alpha} = \int d^3r\left[[\rho_T(\mathbf{r})]_{\gamma\alpha}\varphi^C(\mathbf{r},t) - \frac{1}{c}[\mathbf{J}_T(\mathbf{r})]_{\gamma\alpha}\cdot\mathbf{A}^C(\mathbf{r},t)\right]. \tag{3.1b}$$

If we use Eqs. (2.1a) and (2.1b) to express the differences between the potentials, we get

$$[V^C(t)]_{\gamma\alpha} - [V^L(t)]_{\gamma\alpha} = \int d^3r\left[[\rho_T(\mathbf{r})]_{\gamma\alpha}\left(-\frac{1}{c}\frac{\partial\Lambda(\mathbf{r},t)}{\partial t}\right) - \frac{1}{c}[\mathbf{J}_T(\mathbf{r})]_{\gamma\alpha}\cdot\nabla\Lambda(\mathbf{r},t)\right]. \tag{3.2}$$

Target charge conservation [Eq. (1.4)] plus Gauss's theorem, applied to the localized target charge density, imply that

$$\int[\mathbf{J}_T(\mathbf{r})]_{\gamma\alpha}\cdot\nabla\Lambda(\mathbf{r},t)d^3r = -\int(\nabla\cdot[\mathbf{J}_T(\mathbf{r})]_{\gamma\alpha})\Lambda(\mathbf{r},t)d^3r = i\omega_{\gamma\alpha}\int[\rho_T(\mathbf{r})]_{\gamma\alpha}\Lambda(\mathbf{r},t)d^3r. \tag{3.3}$$

Thus

$$[V^C(t)]_{\gamma\alpha} - [V^L(t)]_{\gamma\alpha} = -\frac{1}{c}\int d^3r[\rho_T(\mathbf{r})]_{\gamma\alpha} \times\left(\frac{\partial\Lambda(\mathbf{r},t)}{\partial t}+i\omega_{\gamma\alpha}\Lambda(\mathbf{r},t)\right). \tag{3.4}$$

A. Point projectile of charge $Z_P e$

If Eqs. (2.3a), (2.5c), and (1.4) are used in the expression (3.1a) for $[V^L(t)]_{\gamma\alpha}$, the result can be written in the form

$$[V^L(t)]_{\gamma\alpha} = Z_P e\int d^3r\,\mathbf{J}_{\gamma\alpha}\cdot\left[\hat{\mathbf{z}}\left(-\frac{(v/c^2)}{\sqrt{\left(\frac{\boldsymbol{\rho}-\mathbf{b}}{\gamma}\right)^2+(vt-z)^2}} + \frac{1}{i\omega_{\gamma\alpha}}\frac{(vt-z)}{\left[\left(\frac{\boldsymbol{\rho}-\mathbf{b}}{\gamma}\right)^2+(vt-z)^2\right]^{3/2}}\right) - \frac{1}{i\omega_{\gamma\alpha}\gamma^2}\frac{\boldsymbol{\rho}-\mathbf{b}}{\left[\left(\frac{\boldsymbol{\rho}-\mathbf{b}}{\gamma}\right)^2+(vt-z)^2\right]^{3/2}}\right]. \tag{3.5}$$

Similarly, $[V^C(t)]_{\gamma\alpha}$ can be obtained by using Eqs. (2.3b), (2.5a), (2.5b), and (1.4) in (3.1b):

$$[V^C(t)]_{\gamma\alpha} = \frac{Z_P e}{v}\int d^3r\,\mathbf{J}_{\gamma\alpha}(\mathbf{r})\cdot\left[\hat{\mathbf{z}}\left(\frac{1}{\gamma^2\sqrt{\frac{|\boldsymbol{\rho}-\mathbf{b}|^2}{\gamma^2}+(z-vt)^2}} - \frac{1}{\sqrt{(\boldsymbol{\rho}-\mathbf{b})^2+(vt-z)^2}}\right) + (\boldsymbol{\rho}-\mathbf{b}) \times\left(\frac{1}{(\boldsymbol{\rho}-\mathbf{b})^2+(vt-z)^2+(vt-z)\sqrt{(\boldsymbol{\rho}-\mathbf{b})^2+(vt-z)^2}} - \frac{1/\gamma^2}{\left(\frac{\boldsymbol{\rho}-\mathbf{b}}{\gamma}\right)^2+(vt-z)^2+(vt-z)\sqrt{\left(\frac{\boldsymbol{\rho}-\mathbf{b}}{\gamma}\right)^2+(vt-z)^2}}\right)\right] + Z_P e\int d^3r\frac{\rho_{\gamma\alpha}}{\sqrt{(\boldsymbol{\rho}-\mathbf{b})^2+(vt-z)^2}}. \tag{3.6}$$

B. Finite spherically symmetric projectile of charge $Z_P e$

If we use $\Lambda(\mathbf{r}, t)$ from Eq. (2.13) in Eq. (3.4), we get

$$[V^C(t)]_{\gamma\alpha} - [V^L(t)]_{\gamma\alpha} = \frac{4}{v}\int_{-\infty}^{\infty} d\omega e^{-i\omega t}\left(\frac{\omega_{\gamma\alpha}}{\omega} - 1\right) \times \int d^3r [\rho_T(\mathbf{r})]_{\gamma\alpha} e^{i\frac{\omega}{v}z}\left[\frac{Z_P e}{4\pi} K_0\left(\frac{|\omega||\boldsymbol{\rho}-\mathbf{b}|}{\gamma v}\right) - K_0\left(\frac{|\omega||\boldsymbol{\rho}-\mathbf{b}|}{v}\right)\int_0^{R_p} r'^2 dr' j_0\left(i\frac{|\omega|}{c}r'\right)\rho_P(r')\right]. \tag{3.7}$$

The time structure of Eq. (3.7) suggests that we formulate the expression in terms of Fourier transforms:

$$V^{C,L}(\omega) \equiv \int_{-\infty}^{\infty}\frac{dt}{\hbar} e^{i\omega t} V^{C,L}(t) \tag{3.8a}$$

$$V^{C,L}(t) \equiv \frac{\hbar}{2\pi}\int_{-\infty}^{\infty} d\omega e^{-i\omega t} V^{C,L}(\omega). \tag{3.8b}$$

Then Eq. (3.7) takes the form

$$[V^C(\omega)]_{\gamma\alpha} - [V^L(\omega)]_{\gamma\alpha} = \frac{8\pi}{\hbar v}\left(\frac{\omega_{\gamma\alpha}}{\omega} - 1\right) \times \int d^3r [\rho_T(\mathbf{r})]_{\gamma\alpha} e^{i\frac{\omega}{v}z}\left[\frac{Z_P e}{4\pi} K_0\left(\frac{|\omega||\boldsymbol{\rho}-\mathbf{b}|}{\gamma v}\right) - K_0\left(\frac{|\omega||\boldsymbol{\rho}-\mathbf{b}|}{v}\right)\int_0^{R_p} r'^2 dr' j_0\left(i\frac{|\omega|}{c}r'\right)\rho_P(r')\right]. \tag{3.9}$$

We see that onshell (i.e., $\omega = \omega_{\gamma\alpha}$) interaction matrix elements are the same in the Coulomb and Lorentz gauges, which confirms the general result obtained in Sec. I concerning the gauge invariance of onshell interaction matrix elements.

To find expressions for $[V^C(\omega)]_{\gamma\alpha}$ and $[V^L(\omega)]_{\gamma\alpha}$ separately, we substitute Eqs. (2.5c) and (2.10) into Eq. (3.1a) and use Eqs. (2.12b), (3.8a), and (3.8b). A straightforward calculation gives

$$[V^L(\omega)]_{\gamma\alpha} = \frac{2Z_P e}{\hbar v}\int d^3r\left[\rho_T(\mathbf{r}) - \frac{v}{c^2}[\mathbf{J}_T(\mathbf{r})]_z\right]_{\gamma\alpha} \times e^{i\frac{\omega}{v}z} K_0\left(\frac{|\omega||\boldsymbol{\rho}-\mathbf{b}|}{\gamma v}\right), \tag{3.10}$$

and then Eq. (3.9) gives

$$[V^C(\omega)]_{\gamma\alpha} = -\frac{2Z_P e}{\hbar c^2}\int d^3r\left[[\mathbf{J}_T]_z - \frac{c^2}{v}\frac{\omega_{\gamma\alpha}}{\omega}\rho_T\right]_{\gamma\alpha} \times e^{i\frac{\omega}{v}z} K_0\left(\frac{|\omega||\boldsymbol{\rho}-\mathbf{b}|}{\gamma v}\right) - \frac{8\pi}{\hbar v}\left(\frac{\omega_{\gamma\alpha}}{\omega} - 1\right) \times \int d^3r [\rho_T(\mathbf{r})]_{\gamma\alpha} e^{i\frac{\omega}{v}z} K_0\left(\frac{|\omega||\boldsymbol{\rho}-\mathbf{b}|}{v}\right) \times \int_0^{R_p} r'^2 dr' j_0\left(i\frac{|\omega|}{c}r'\right)\rho_P(r'). \tag{3.11}$$

Finally we can proceed, as in Eq. (3.6), to express the matrix elements in terms of the current density only:

$$[V^L(\omega)]_{\gamma\alpha} = -\frac{2Z_P e}{\hbar c^2}\int d^3r [\mathbf{J}_T(\mathbf{r})]_{\gamma\alpha}\cdot\left(\hat{\mathbf{z}} + \frac{ic^2}{v\omega_{\gamma\alpha}}\nabla\right) \times e^{i\frac{\omega}{v}z} K_0\left(\frac{|\omega||\boldsymbol{\rho}-\mathbf{b}|}{\gamma v}\right) \tag{3.12a}$$

$$[V^C(\omega)]_{\gamma\alpha} = -\frac{2Z_P e}{\hbar c^2}\int d^3r [\mathbf{J}_T(\mathbf{r})]_{\gamma\alpha}\cdot\left(\hat{\mathbf{z}} + \frac{ic^2}{v\omega}\nabla\right) \times e^{i\frac{\omega}{v}z} K_0\left(\frac{|\omega||\boldsymbol{\rho}-\mathbf{b}|}{\gamma v}\right) - \frac{8\pi i}{v\hbar\omega_{\gamma\alpha}}\left(1 - \frac{\omega_{\gamma\alpha}}{\omega}\right) \times \int_0^{R_p} r'^2 dr' j_0\left(i\frac{|\omega|}{c}r'\right)\rho_P(r') \times \int d^3r [\mathbf{J}_T(\mathbf{r})]_{\gamma\alpha}\cdot\nabla e^{i\frac{\omega}{v}z} K_0\left(\frac{|\omega||\boldsymbol{\rho}-\mathbf{b}|}{v}\right). \tag{3.12b}$$

In the following sections, we investigate significant differences between expressions (3.12a) and (3.12b).

IV. COMPARISON OF THE STRUCTURES OF $V^L(\omega)$ AND $V^C(\omega)$

A. High bombarding energy limits

At high bombarding energy, where $v \sim c$, the main bombarding energy dependence enters $V^L(\omega)$ and $V^C(\omega)$ via the γ dependencies exhibited by Eqs. (3.12a) and (3.12b). Since

$$\lim_{\substack{\gamma\to\infty\\ v\to c}} K_0\left(\frac{|\omega||\boldsymbol{\rho}-\mathbf{b}|}{\gamma v}\right) = -\log\left(\frac{|\omega||\boldsymbol{\rho}-\mathbf{b}|}{\gamma c}\right) \overset{\gamma\to\infty}{\longrightarrow} \log\gamma,$$

we have

$$\lim_{\substack{\gamma\to\infty\\ v\to c}} [V^L(\omega)]_{\gamma\alpha} = -\frac{2Z_P e}{\hbar c^2}\log\gamma \times \int d^3r [\mathbf{J}_T(\mathbf{r})]_{\gamma\alpha}\cdot\left[\hat{\mathbf{z}} + \frac{ic^2}{v\omega_{\gamma\alpha}}\nabla\right] e^{i\frac{\omega}{v}z} = -\frac{2Z_P e}{\hbar c^2}\log\gamma\left(1 - \frac{\omega}{\omega_{\gamma\alpha}}\frac{c^2}{v^2}\right)\int d^3r [\mathbf{J}_T(\mathbf{r})]_{\gamma\alpha}\cdot\hat{\mathbf{z}} e^{i\frac{\omega}{v}z} \overset{v\to c}{\longrightarrow} -\frac{2Z_P e}{\hbar c^2}\log\gamma\left(1 - \frac{\omega}{\omega_{\gamma\alpha}}\right)\int d^3r [\mathbf{J}_T(\mathbf{r})]_{\gamma\alpha}\cdot\hat{\mathbf{z}} e^{i\frac{\omega}{v}z}. \tag{4.1}$$

Since the ϕ dependence of $[\mathbf{J}_T(\mathbf{r})]_{\gamma\alpha}\cdot\hat{\mathbf{z}}$ is given by $e^{i(M_\gamma - M_\alpha)\phi}$, the axial symmetry of $e^{i\frac{\omega}{v}z}$ implies that the integral in (4.1) vanishes unless $M_\gamma - M_\alpha(\equiv\mu) = 0$. Thus we can have a $\log\gamma$ divergence of $[V^L(\omega)]_{\gamma\alpha}$ if $\omega \neq \omega_{\gamma\alpha}$ and $M_\gamma = M_\alpha$. The effect of this divergence on high bombarding energy cross sections was noted in Ref. [11] and is illustrated in Sec. VI below.

The high-bombarding-energy behavior of $[V^C(\omega)]_{\gamma\alpha}$ is quite different. The last two lines of Eq. (3.12b) are independent of γ and so obviously do not diverge as $\gamma \to \infty$. The high-γ behavior of the first line is dominated by

$$\lim_{\substack{\gamma\to\infty\\ v\to c}} -\frac{2Z_P e}{\hbar c^2}\log\gamma\int d^3r[\mathbf{J}_T(\mathbf{r})]_{\gamma\alpha}\cdot\left[\hat{\mathbf{z}}+\frac{ic^2}{v\omega}\nabla\right]e^{i\frac{\omega}{v}z}$$
$$=-\frac{2Z_P e}{\hbar c^2}\log\gamma\left(1-\frac{c^2}{v^2}\right)\int d^3r[\mathbf{J}_T(\mathbf{r})]_{\gamma\alpha}\cdot\hat{\mathbf{z}}e^{i\frac{\omega}{v}z}$$
$$=\frac{2Z_P e}{\hbar v^2}\frac{\log\gamma}{\gamma^2}\int d^3r[\mathbf{J}_T(\mathbf{r})]_{\gamma\alpha}\cdot\hat{\mathbf{z}}e^{i\frac{\omega}{v}z}.$$

The factor of $1/\gamma^2$ overpowers the $\log\gamma$ divergence, and the matrix element $[V^C(\omega)]_{\gamma\alpha}$ is seen to be finite at arbitrarily high bombarding energy.

B. Multipole expansions of $V^L(\omega)$ and $V^C(\omega)$

It is illuminating to express Eqs. (3.12a) and (3.12b) in terms of the multipole expansion given by WA, which is

$$e^{i\frac{\omega}{v}z}K_0\left(\frac{|\omega||\boldsymbol{\rho}-\mathbf{b}|}{\gamma v}\right)=\sum_\mu e^{-i\mu\phi_{\mathbf{b}}}K_\mu\left(\frac{|\omega|b}{\gamma v}\right)\times\sum_\lambda\mathcal{G}_{\lambda\mu}j_\lambda\left(\frac{|\omega|}{c}r\right)Y^\lambda_\mu(\hat{\mathbf{r}}) \tag{4.2a}$$

with $\mathcal{G}_{\lambda\mu}$ defined by

$$\mathcal{G}_{\lambda\mu}\equiv\frac{i^{\lambda+\mu}}{(2\gamma)^\mu}\left(\frac{\omega}{|\omega|}\right)^{\lambda-\mu}\left(\frac{c}{v}\right)^\lambda\sqrt{4\pi(2\lambda+1)(\lambda-\mu)!(\lambda+\mu)!}\times\sum_n\frac{1}{(2\gamma)^{2n}(n+\mu)!n!(\lambda-\mu-2n)!}. \tag{4.2b}$$

To expand the third line of Eq. (3.12b), we also need the $\gamma\to 1$ limits of Eqs. (4.2a) and (4.2b). To perform these limits, without affecting the value of v, we allow $c\to\infty$ and obtain

$$e^{i\frac{\omega}{v}z}K_0\left(\frac{|\omega||\boldsymbol{\rho}-\mathbf{b}|}{v}\right)=\sum_\mu e^{-i\mu\phi_{\mathbf{b}}}K_\mu\left(\frac{|\omega|b}{v}\right)\times\sum_\lambda\sqrt{\frac{4\pi}{2\lambda+1}}\frac{i^{\lambda+\mu}}{\sqrt{(\lambda+\mu)!(\lambda-\mu)!}}\left(\frac{|\omega|}{\omega}\right)^{\lambda-\mu}\left(\frac{\omega r}{v}\right)^\lambda Y^\lambda_\mu(\hat{\mathbf{r}}). \tag{4.3}$$

If we apply Eqs. (4.2a) and (4.3) to Eq. (3.12b), we find

$$[V^C(\omega)]_{\gamma\alpha}=\frac{2Z_P e}{\hbar v}\sum_\mu e^{-i\mu\phi_b}\cdot\sum_{\lambda=|\mu|}^\infty\left[\left(X^\lambda_\mu(E)+X^\lambda_\mu(M)\right)\times K_\mu\left(\frac{|\omega|b}{\gamma v}\right)+X^\lambda_\mu(S)K_\mu\left(\frac{|\omega|b}{v}\right)\right], \tag{4.4}$$

where

$$X^\lambda_\mu(E)\equiv\frac{iv}{c\hbar\omega}\left[\frac{\mathcal{G}_{\lambda-1,\mu}}{\lambda}\sqrt{\frac{\lambda^2-\mu^2}{(2\lambda+1)(2\lambda-1)}}+\frac{\mathcal{G}_{\lambda+1,\mu}}{\lambda+1}\sqrt{\frac{(\lambda+1)^2-\mu^2}{(2\lambda+1)(2\lambda+3)}}\right]\times\int d^3r[\mathbf{J}_T]_{\gamma\alpha}(\mathbf{r})\cdot(\nabla\times\mathbf{L})j_\lambda\left(\frac{\omega}{c}r\right)Y^\lambda_\mu(\hat{\mathbf{r}}) \tag{4.5a}$$

$$X^\lambda_\mu(M)\equiv-\frac{v\mu}{c^2\hbar}\frac{\mathcal{G}_{\lambda,\mu}}{\lambda(\lambda+1)}\int d^3r[\mathbf{J}_T]_{\gamma\alpha}(\mathbf{r})\cdot\mathbf{L}j_\lambda\left(\frac{\omega}{c}r\right)Y^\lambda_\mu(\hat{\mathbf{r}}) \tag{4.5b}$$

$$X^\lambda_\mu(S)\equiv\left(1-\frac{\omega_{\gamma\alpha}}{\omega}\right)\frac{4\pi}{Z_P e}\int_0^\infty\tilde{r}^2d\tilde{r}\,\tilde{\rho}_P(\tilde{r})j_0\left(i\tilde{r}\frac{\omega}{c}\right)\times\sqrt{\frac{4\pi}{2\lambda+1}}\frac{i^{\lambda+\mu}}{\sqrt{(\lambda+\mu)!(\lambda-\mu)!}}\left(\frac{|\omega|}{\omega}\right)^{\lambda-\mu}\times\frac{1}{i\omega_{\gamma\alpha}}\left(\frac{\omega}{v}\right)^\lambda\times\int d^3r[\mathbf{J}_T(\mathbf{r})]_{\gamma\alpha}\cdot\nabla r^\lambda Y^\lambda_\mu(\hat{\mathbf{r}}). \tag{4.5c}$$

On the other hand, substituting Eq. (4.2a) into Eq. (3.12a) gives

$$[V^L(\omega)]_{\gamma\alpha}=\frac{2Z_P e}{\hbar v}\sum_\mu e^{-i\mu\phi_{\mathbf{b}}}\cdot\sum_{\lambda=|\mu|}^\infty\left[X^\lambda_\mu(E)+X^\lambda_\mu(M)+X^\lambda_\mu(G)\right]K_\mu\left(\frac{|\omega|b}{\gamma v}\right). \tag{4.6}$$

$X^\lambda_\mu(E)$ and $X^\lambda_\mu(M)$ in Eq. (4.6) are the same as in Eqs. (4.5a) and (4.5b), but $X^\lambda_\mu(G)$ is defined by

$$X^\lambda_\mu(G)\equiv\left(1-\frac{\omega_{\gamma\alpha}}{\omega}\right)\frac{\mathcal{G}_{\lambda\mu}}{i\omega_{\gamma\alpha}}\times\int d^3r[\mathbf{J}_T(\mathbf{r})]_{\gamma\alpha}\cdot\nabla j_\lambda\left(\frac{|\omega|}{c}r\right)Y^\lambda_\mu(\hat{\mathbf{r}}). \tag{4.7}$$

C. Monopole matrix elements

Inspection of Eqs. (4.4) and (4.5a)–(4.5c) shows that $[V^C(\omega)]_{\gamma\alpha}$ can be expressed as

$$[V^C(\omega)]_{\gamma\alpha}=\int d^3r[\mathbf{J}_T(\mathbf{r})]_{\gamma\alpha}\cdot\mathbf{Q}^C(\mathbf{r}), \tag{4.8}$$

where $\mathbf{Q}^C(\mathbf{r})$ is a linear combination of $(\nabla\times\mathbf{L})j_\lambda(\frac{\omega}{c}r)Y^\lambda_\mu(\hat{\mathbf{r}})$, $\mathbf{L}j_\lambda(\frac{\omega}{c}r)Y^\lambda_\mu(\hat{\mathbf{r}})$, and $\nabla r^\lambda Y^\lambda_\mu(\hat{\mathbf{r}})$. Since

$$\nabla\cdot(\nabla\times\mathbf{L})j_\lambda\left(\tfrac{\omega}{c}r\right)Y^\lambda_\mu(\hat{\mathbf{r}})=0,$$
$$\nabla\cdot\mathbf{L}j_\lambda\left(\tfrac{\omega}{c}r\right)Y^\lambda_\mu(\hat{\mathbf{r}})=0,\quad\text{and}\quad\nabla\cdot\nabla r^\lambda Y^\lambda_\mu(\hat{\mathbf{r}})=0,$$

it follows that

$$\nabla\cdot\mathbf{Q}^C(\mathbf{r})=0. \tag{4.9}$$

Now suppose that ϕ_α and ϕ_γ are both states of total angular momentum zero ($J=0$). Then $[\mathbf{J}_T(\mathbf{r})]_{\gamma\alpha}$ is a spherically symmetric vector field (a *central* field) and can be written as the gradient of a spherically symmetric scalar field:

$$[\mathbf{J}_T(\mathbf{r})]_{\gamma\alpha}=\nabla\psi(r).$$

Equations (4.8) and (4.9) imply that

$$[V^C(\omega)]_{\gamma\alpha}=\int d^3r\nabla\psi(r)\cdot\mathbf{Q}^C(\mathbf{r})=-\int d^3r\,\psi(r)\nabla\cdot\mathbf{Q}^C(\mathbf{r})=0,$$

so that the matrix elements of V^C between any two $J = 0$ states vanish identically. Thus an excited $J = 0$ state, in a nucleus with a $J = 0$ ground state, can only be populated indirectly, via a multistep process. However, if $[V^L(\omega)]_{\gamma\alpha}$ is expressed as

$$[V^L(\omega)]_{\gamma\alpha} = \int d^3r [\mathbf{J}_T(\mathbf{r})]_{\gamma\alpha} \cdot \mathbf{Q}^L(\mathbf{r}), \tag{4.10}$$

then one of the components in the expansion of $\mathbf{Q}^L(\mathbf{r})$ is $\nabla j_\lambda(|\omega|r/c)Y^\lambda_\mu(\hat{\mathbf{r}})$ [see Eqs. (4.6) and (4.7)]. But

$$\nabla \cdot \nabla j_\lambda \left(\frac{|\omega|}{c} r\right) Y^\lambda_\mu(\hat{\mathbf{r}}) = \nabla^2 j_\lambda \left(\frac{|\omega|}{c} r\right) Y^\lambda_\mu(\hat{\mathbf{r}})$$
$$= -\left(\frac{\omega}{c}\right)^2 j_\lambda \left(\frac{|\omega|}{c} r\right) Y^\lambda_\mu(\hat{\mathbf{r}}),$$

which is not identically zero. Thus $\nabla \cdot \mathbf{Q}^L(\mathbf{r})$ is not identically zero, and there is no reason to expect matrix elements of V^L between $J = 0$ states to vanish. A calculation based on V^L implies the possibility of one-step population of an excited $J = 0$ state from a $J = 0$ ground state.

V. NUMERICAL COMPARISONS OF MATRIX ELEMENTS OF V^L AND V^C

The following numerical comparisons refer to Coulomb excitation of the giant dipole resonance (GDR) in a ^{40}Ca target by a ^{208}Pb projectile. The target transition current density matrix elements $[\mathbf{J}_T(\mathbf{r})]_{\gamma\alpha}$ needed in Eqs. (4.5) and (4.7) are calculated using Brink's model [15] of the GDR, in which unexcited proton and neutron spheres undergo harmonic oscillations relative to each other. The radial densities of the spheres are obtained by filling the lowest available shell-model single-particle states. The relative harmonic oscillations of the proton and neutrons spheres are characterized by the eigenstates $\phi^{n,\ell}_m(\mathbf{r}_{\rm pn})$ of a three-dimensional harmonic oscillator. The ground state is $\phi^{0,0}_0$. The degenerate first excited states that can be populated by Coulomb excitation are $\phi^{0,1}_0$ and $(\phi^{0,1}_1 + \phi^{0,1}_{-1})/\sqrt{2}$, the combination of $\phi^{0,1}_{\pm 1}$ symmetric under reflection across the reaction plane. Further details on the calculation of matrix elements using the Brink model eigenstates are given in Ref. [11].

In the calculations represented in Fig. 1, it has been assumed that the 82 protons of ^{208}Pb are distributed uniformly within a sphere of radius 7.5 fm (as seen by an observer moving with the projectile). The parameters used for the calculations imply that $b = 20$ fm and $\omega_{\gamma\alpha} = 11.7$ MeV/$\hbar$. It can be verified by inspection of Fig. 1 that, in every case, V^C and V^L agree at $\omega = 11.7$ MeV/$\hbar$, as required by Eq. (3.9).

In Fig. 1, $\mu = 0$ refers to the transition $\phi^{0,0}_0 \to \phi^{0,1}_0$, and $\mu = 1$ refers to the transition $\phi^{0,0}_0 \to (\phi^{0,1}_1 + \phi^{0,1}_{-1})/\sqrt{2}$. In every case, the solid line gives $V^C(\omega)$, whereas the dashed line gives $V^L(\omega)$.

The first observation concerning Fig. 1 is that at a bombarding energy of $E/A = 100$ MeV, there is little difference between V^C and V^L. However, at $E/A = 10$ GeV, the difference is pronounced. The most striking difference is the very strong increase with bombarding energy of V^L for the $\mu = 0$ transition. This is an expression of the logarithmic divergence (with increasing γ) of the $\mu = 0$ matrix elements of V^L, as shown in Eq. (4.1). It is clear that, at high bombarding energy, calculations using V^L ascribe a much higher role to $\mu = 0$ transitions than do calculations using V^C.

Figure 1 also shows that, at high bombarding energy, the use of the Coulomb gauge leads to an interaction that is more adiabatic than predicted by the Lorentz gauge. The wider spread of $V^L(\omega)$, as a function of ω, compared to the spread of $V^C(\omega)$, shows that the impulse in the Lorentz gauge is sharper than the Coulomb gauge impulse. For example, Fig. 2 shows the same comparison as in the $E/A = 10$ GeV, $\mu = 1$ plot of Fig. 1, but in the time domain. The sharpness of the pulse provided by $V^L(t)$, compared with that provided by $V^C(t)$, is evident. Note that in this particular case, $[V^L(-\omega)]_{\gamma\alpha} = [V^L(\omega)]_{\gamma\alpha}$, which has the consequence that $[V^L(t)]_{\gamma\alpha}$ is real. However, this is not true of $[V^C(\omega)]_{\gamma\alpha}$, and thus $[V^C(t)]_{\gamma\alpha}$ has both real and imaginary parts.

VI. GAUGE-DEPENDENT EFFECTS IN COUPLED-CHANNEL CALCULATIONS

The most significant test of the differences between V^L and V^C is in the calculation of relativistic Coulomb excitation (RCE) cross sections, since the cross section is the point where theory and experiment intersect. In this section, we compare cross sections calculated with these two interactions, for the ^{208}Pb + ^{40}Ca system described in Sec. V. We have performed coupled-channel integrations of the time-dependent Schrödinger equation. The target states included in the calculation span were the zero-phonon, one-phonon, and two-phonon states of the ^{40}Ca GDR. The methods used to do the numerical Fourier transform needed in Eq. (3.8b), and to integrate the coupled equations, are described in Ref. [11]. We also describe there the integrations over the impact parameter needed to calculate the cross section.

Figure 3 compares the calculated cross sections for the population of the six reflection-symmetric one- and two-phonon states that can be reached via RCE, as functions of the kinetic energy of the ^{208}Pb projectile nucleus. In every case, a solid line is used to show the result of the calculation using $V^C(t)$, and a dashed line is used to show the result of the corresponding calculation using $V^L(t)$.

For the one-phonon states, the situation is similar to that shown in Fig. 1. The two sets of calculations agree at low bombarding energy ($E/A \gtrsim 1$ GeV). However, at high bombarding energy ($E/A \gtrsim 5$ GeV), $V^L(t)$ predicts much greater cross sections for the population of the $J = 1$, $M = 0$ state than does $V^C(t)$. The situation is more complicated for the two-phonon states. The cross sections are much smaller than for the one-phonon states, and they depend upon multiple excitation processes. Also, the truncation of our calculation at two phonons introduces an additional element of uncertainty into our two-phonon cross sections. However, it is noteworthy that the two-phonon $|M| = 1$ state is also strongly favored by $V^L(t)$ at high bombarding energy, compared to $V^C(t)$. The reason is that this state is mostly populated in two-step

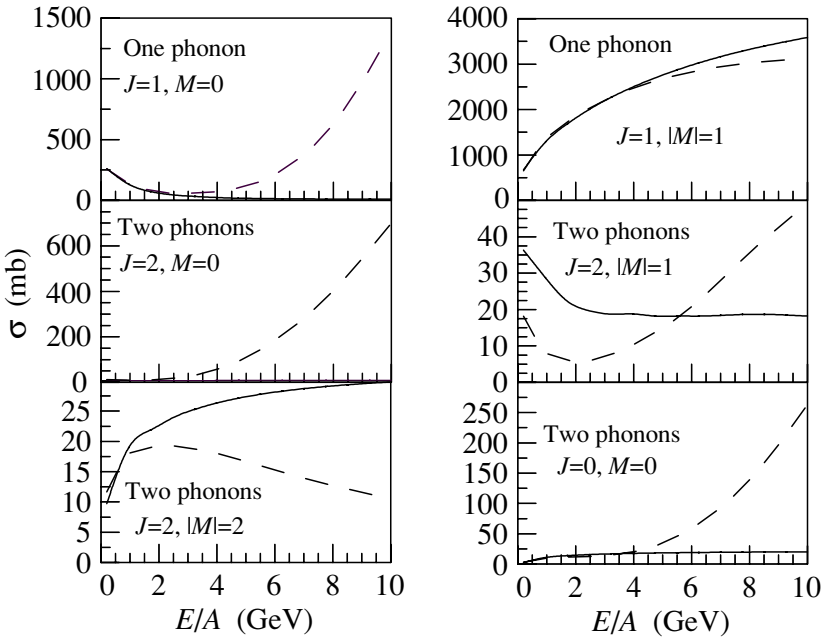

FIG. 3. Calculated coupled-channel Coulomb excitation cross sections for one- and two-phonon states of the GDR in ^{40}Ca with ^{208}Pb projectiles. The solid curves correspond to calculations in which the Coulomb gauge has been used; the dashed curves correspond to calculations with the Lorentz gauge.

processes, such as

$$(J = M = 0) \rightarrow (J = 1, M = 0) \rightarrow (J = 2, |M| = 1)$$

and

$$(J = M = 0) \rightarrow (J = 1, |M| = 1) \rightarrow (J = 2, |M| = 1).$$

In both cases, a $\Delta M = 0$ transition is involved, and it is the logarithmic divergence (with increasing γ) of the $\Delta M = 0$ transition amplitude that leads to the strongly increasing cross section when $V^L(t)$ is used. But the $J = 2, |M| = 2$ state is reached mainly by

$$(J = M = 0) \rightarrow (J = 1, |M| = 1) \rightarrow (J = 2, |M| = 2),$$

in which there is no $\Delta M = 0$ step, and so the $J = 2, |M| = 2$ state is not strongly favored by $V^L(t)$ at high bombarding energy. Thus we see that for $E/A \gtrsim 5$ GeV, $V^C(t)$ and $V^L(t)$ predict very different cross sections when used in truncated coupled-channel analyses. A calculation using $V^L(t)$ will predict stongly enhanced cross sections for populating any state that can be reached via a one-step or two-step process involving a $\Delta M = 0$ transition.

The stongest transition illustrated in Fig. 3 populates the one-phonon $|M| = 1$ state. It is predominantly a one-step transition and so is well described by the Born approximation. According to Eq. (4.4) or (4.6), this implies that the b dependence of the transition probability is given by

$$\left[K_1\left(\frac{\omega_{\text{on-shell}}b}{\gamma v}\right)\right]^2$$

whose the integral over the impact parameter diverges in the $\gamma \rightarrow \infty$ limit [cf. Eqs. (3.1) and (3.6) of Ref. [2]]. The physical reason for this divergence is that as γ increases and the electromagnetic pulse becomes more strongly retarded, it becomes flatter and its influence extends for a longer distance away from the trajectory of the projectile. Thus, in the integral over b, larger values of b play a more important role as γ increases, and in the $\gamma \rightarrow \infty$ limit, the b integral diverges. This occurs only for $\Delta M = \pm 1$, because the flat pulse is spatially axially symmetric ($\Delta M = 0$) and the intrinsic spin of the photon transfers $\Delta M = \pm 1$. The one-phonon $|M| = 1$ cross section shown in Fig. 3 exhibits this logarithmic-like increase with bombarding energy.

However, the log γ divergence of the offshell $\mu = \Delta M = 0$ matrix element, discussed in Section IV A, is a much more serious divergence. It occurs for *every* b, and thus the b-integrated cross section would be a divergence of still higher order. This is the divergence that is introduced when the Lorentz gauge is used in a coupled-channel calculation, a divergence that is not present when the Coulomb gauge is used.

The expression for $V^L(\omega)$ given by Eq. (3.12a) depends upon the total projectile charge but not on the radial dependence of this charge. However, there *is* a dependence on the projectile radial charge density in $V^C(\omega)$ given by Eq. (3.12b). Fortunately, this dependence is very weak. The calculations using $V^C(\omega)$ whose results are shown in Fig. 3 were done using a radial charge distribution that was constant from the center out to 7.5 fm. By way of comparison, we have repeated these calculations, assuming that the entire charge of the ^{208}Pb nucleus is concentrated at its center. In all cases, we found that the calculated cross sections changed by no more than a few tenths of a percent. As might be expected, the transition amplitudes are more sensitive to projectile radial density at small impact parameters. However, when the integration over all impact parameters is done, the residual effect on the cross section of changes in the projectile radial charge density is very small.

VII. CONCLUSIONS AND DISCUSSION

We have studied the relationship between the electromagnetic potentials in the Lorentz gauge and the Coulomb gauge

for the fields encountered in relativistic Coulomb excitation and have found expressions in the two gauges for the interaction between projectile and target. At bombarding energies above about 2 GeV per nucleon we have found significant differences in excitation cross sections when the two gauges are used in coupled-channel time-dependent calculations, especially for processes involving $\Delta M = 0$ transitions. Since there is no *a priori* reason for using one gauge rather than another, this lack of gauge invariance reveals a weakness of the coupled-channel time-dependent approach to relativistic Coulomb excitation. It demonstrates that the common practice of relying totally on calculations in the Lorentz gauge cannot be justified.

We have discussed one cause of lack of gauge invariance, the truncation of the set of target states used in the coupled-channel calculation. Another cause is revealed by consideration of the Hamiltonian for a target charged particle moving in the fields ($\varphi(\mathbf{r}, t)$, $\mathbf{A}(\mathbf{r}, t)$) produced by the projectile:

$$\begin{aligned} H &= \frac{1}{2m}\left(\mathbf{p} - \frac{e\mathbf{A}(\mathbf{r}, t)}{c}\right)^2 + e\varphi(\mathbf{r}, t) + U_{\text{nuc}}(\mathbf{r}) \\ &= \frac{1}{2m}\mathbf{p}^2 - \frac{e}{2mc}(\mathbf{p}\cdot\mathbf{A}(\mathbf{r}, t) + \mathbf{A}(\mathbf{r}, t)\cdot\mathbf{p}) + e\varphi(\mathbf{r}, t) \\ &\quad + \frac{e^2}{2mc^2}\mathbf{A}(\mathbf{r}, t)\cdot\mathbf{A}(\mathbf{r}, t) + U_{\text{nuc}}(\mathbf{r}). \end{aligned} \tag{7.1}$$

The terms in Eq. (7.1) that are linear in e,

$$-\frac{e}{2mc}(\mathbf{p}\cdot\mathbf{A}(\mathbf{r}, t) + \mathbf{A}(\mathbf{r}, t)\cdot\mathbf{p}) + e\varphi(\mathbf{r}, t),$$

give rise to the interaction (1.3) that has been the basis of this study. However, the term quadratic in e,

$$\frac{e^2}{2mc^2}\mathbf{A}(\mathbf{r}, t)\cdot\mathbf{A}(\mathbf{r}, t),$$

has not been included in our calculation, or in other studies published to date on relativistic Coulomb excitation. But the equation

$$\begin{aligned} &\left(\mathbf{p} - \frac{e(\mathbf{A}(\mathbf{r}, t) + \nabla\Lambda(\mathbf{r}, t))}{c}\right)^2 e^{i\frac{e\Lambda(\mathbf{r},t)}{\hbar c}}\psi(\mathbf{r}, t) \\ &\quad = e^{i\frac{e\Lambda(\mathbf{r},t)}{\hbar c}}\left(\mathbf{p} - \frac{e\mathbf{A}(\mathbf{r}, t)}{c}\right)^2\psi(\mathbf{r}, t), \end{aligned}$$

which is an essential component in the argument about the gauge invariance of the observable consequences of the Schrödinger equation, relies for its validity on the presence of the $\mathbf{A}\cdot\mathbf{A}$ term. Thus it is clear that no gauge invariant theory of relativistic Coulomb excitation can be constructed without inclusion of this term. We will address this issue in a forthcoming publication.

APPENDIX: TWO INTEGRAL RELATIONS

Define $I(\tilde{r})$ by

$$I(\tilde{r}) \equiv \int \frac{d^2\mathbf{q}_\perp}{q_\perp^2 + \lambda_1^2} e^{i\mathbf{q}_\perp\cdot(\boldsymbol{\rho}-\mathbf{b})} j_0\big(\tilde{r}\sqrt{q_\perp^2 + \lambda_2^2}\big). \tag{A1}$$

Operate on this expression with $\nabla_{\tilde{\mathbf{r}}}^2$:

$$\begin{aligned} \nabla_{\tilde{\mathbf{r}}}^2 I(\tilde{r}) &= \int \frac{d^2\mathbf{q}_\perp}{q_\perp^2 + \lambda_1^2} e^{i\mathbf{q}_\perp\cdot(\boldsymbol{\rho}-\mathbf{b})} \nabla_{\tilde{\mathbf{r}}}^2 j_0\big(\tilde{r}\sqrt{q_\perp^2 + \lambda_2^2}\big) \\ &= -\int d^2\mathbf{q}_\perp \frac{q_\perp^2 + \lambda_2^2}{q_\perp^2 + \lambda_1^2} e^{i\mathbf{q}_\perp\cdot(\boldsymbol{\rho}-\mathbf{b})} j_0\big(\tilde{r}\sqrt{q_\perp^2 + \lambda_2^2}\big) \\ &= -\int d^2\mathbf{q}_\perp \left(1 + \frac{\lambda_2^2 - \lambda_1^2}{q_\perp^2 + \lambda_1^2}\right) e^{i\mathbf{q}_\perp\cdot(\boldsymbol{\rho}-\mathbf{b})} j_0\big(\tilde{r}\sqrt{q_\perp^2 + \lambda_2^2}\big) \\ &= -\int d^2\mathbf{q}_\perp e^{i\mathbf{q}_\perp\cdot(\boldsymbol{\rho}-\mathbf{b})} j_0\big(\tilde{r}\sqrt{q_\perp^2 + \lambda_2^2}\big) \\ &\quad - \big(\lambda_2^2 - \lambda_1^2\big)\int \frac{d^2\mathbf{q}_\perp}{q_\perp^2 + \lambda_1^2} e^{i\mathbf{q}_\perp\cdot(\boldsymbol{\rho}-\mathbf{b})} j_0\big(\tilde{r}\sqrt{q_\perp^2 + \lambda_2^2}\big). \end{aligned} \tag{A2}$$

In the first term of Eq. (A2), replace $j_0(\tilde{r}\sqrt{q_\perp^2 + \lambda_2^2})$ by

$$j_0\big(\tilde{r}\sqrt{q_\perp^2 + \lambda_2^2}\big) = \frac{1}{4\pi}\int \sin\tilde{\theta}\, d\tilde{\theta}\, d\tilde{\phi}\, e^{-i(\mathbf{q}_\perp\cdot\tilde{\boldsymbol{\rho}} + \lambda_2\tilde{z})},$$

where $\tilde{\boldsymbol{\rho}} \equiv \tilde{r}\sin\tilde{\theta}(\cos\tilde{\phi}\,\hat{\mathbf{x}} + \sin\tilde{\phi}\,\hat{\mathbf{y}})$ and $\tilde{z} = \tilde{r}\cos\tilde{\theta}$. Then Eq. (A2) becomes

$$\begin{aligned} \nabla_{\tilde{\mathbf{r}}}^2 I(\tilde{r}) &= -\frac{1}{4\pi}\int \sin\tilde{\theta}\, d\tilde{\theta}\, d\tilde{\phi} \int d^2\mathbf{q}_\perp e^{i\mathbf{q}_\perp\cdot(\boldsymbol{\rho}-\mathbf{b}-\tilde{\boldsymbol{\rho}})} e^{-i\lambda_2\tilde{z}} \\ &\quad - \big(\lambda_2^2 - \lambda_1^2\big)\int \frac{d^2\mathbf{q}_\perp}{q_\perp^2 + \lambda_1^2} e^{i\mathbf{q}_\perp\cdot(\boldsymbol{\rho}-\mathbf{b})} j_0\big(\tilde{r}\sqrt{q_\perp^2 + \lambda_2^2}\big) \\ \nabla_{\tilde{\mathbf{r}}}^2 I(\tilde{r}) + \big(\lambda_2^2 - \lambda_1^2\big) I(\tilde{r}) &= -\frac{(2\pi)^2}{4\pi} \\ &\quad \times \int \sin\tilde{\theta}\, d\tilde{\theta}\, d\tilde{\phi}\, e^{-i\lambda_2\tilde{z}} \delta(\boldsymbol{\rho} - \mathbf{b} - \tilde{\boldsymbol{\rho}}). \end{aligned} \tag{A3}$$

In our application, $|\boldsymbol{\rho}|$ is bounded by the radius of the target and $|\tilde{\boldsymbol{\rho}}|$ is bounded by the radius of the projectile. The condition that the projectile and target do not overlap implies that $|\boldsymbol{\rho} - \mathbf{b}| > |\tilde{\boldsymbol{\rho}}|$ for every orientation $\tilde{\theta}$, $\tilde{\phi}$, and so $\boldsymbol{\rho} - \mathbf{b} - \tilde{\boldsymbol{\rho}}$ is never zero. Thus the δ function on the right-hand side of Eq. (A3) vanishes, and we get

$$\nabla_{\tilde{\mathbf{r}}}^2 I(\tilde{r}) + \big(\lambda_2^2 - \lambda_1^2\big) I(\tilde{r}) = 0. \tag{A4}$$

We have two applications of Eq. (A4). In one of them, $\lambda_1^2 = \lambda_2^2 = (\omega/(\gamma v))^2$. In the other, $\lambda_1^2 = (\omega/v)^2$, $\lambda_2^2 = (\omega/(\gamma v))^2$. Thus in both cases $(\lambda_2^2 - \lambda_1^2) \leqslant 0$, and we can write the general solution of Eq. (A4) as

$$I(\tilde{r}) = \alpha\, j_0\big(i\tilde{r}\sqrt{\lambda_1^2 - \lambda_2^2}\big) + \beta\, n_0\big(i\tilde{r}\sqrt{\lambda_1^2 - \lambda_2^2}\big), \tag{A5}$$

where α and β are independent of $\tilde{r}$. The first term in Eq. (A5) is finite at $\tilde{r} = 0$, whereas the second term diverges there. But if we set $\tilde{r} = 0$ in the definition (A1), we get

$$I(0) = \int \frac{d^2\mathbf{q}_\perp}{q_\perp^2 + \lambda_1^2} e^{i\mathbf{q}_\perp\cdot(\boldsymbol{\rho}-\mathbf{b})} = 2\pi\, K_0(|\lambda_1||\boldsymbol{\rho} - \mathbf{b}|), \tag{A6}$$

which is finite in our $|\boldsymbol{\rho} - \mathbf{b}| \geqslant 0$ situation. Thus β in Eq. (A5) vanishes and

$$I(0) = \alpha j_0(0) = \alpha = 2\pi K_0(|\lambda_1||\boldsymbol{\rho} - \mathbf{b}|),$$

leading to

$$I(\tilde{r}) \equiv \int \frac{d^2\mathbf{q}_\perp}{q_\perp^2 + \lambda_1^2} e^{i\mathbf{q}_\perp\cdot(\boldsymbol{\rho}-\mathbf{b})} j_0\big(\tilde{r}\sqrt{q_\perp^2 + \lambda_2^2}\big) = 2\pi K_0(|\lambda_1||\boldsymbol{\rho} - \mathbf{b}|) j_0\big(i\tilde{r}\sqrt{\lambda_1^2 - \lambda_2^2}\big). \tag{A7}$$

Thus we get the two special cases

$$\int \frac{d^2\mathbf{q}_\perp}{q_\perp^2 + \left(\frac{\omega}{\gamma v}\right)^2} e^{i\mathbf{q}_\perp\cdot(\boldsymbol{\rho}-\mathbf{b})} j_0\left(\tilde{r}\sqrt{q_\perp^2 + \left(\frac{\omega}{\gamma v}\right)^2}\right) = 2\pi K_0\left(\frac{|\omega||\boldsymbol{\rho} - \mathbf{b}|}{\gamma v}\right) \tag{A8a}$$

$$\int \frac{d^2\mathbf{q}_\perp}{q_\perp^2 + \left(\frac{\omega}{v}\right)^2} e^{i\mathbf{q}_\perp\cdot(\boldsymbol{\rho}-\mathbf{b})} j_0\left(\tilde{r}\sqrt{q_\perp^2 + \left(\frac{\omega}{\gamma v}\right)^2}\right) = 2\pi K_0\left(\frac{|\omega||\boldsymbol{\rho} - \mathbf{b}|}{v}\right) j_0\left(i\tilde{r}\frac{|\omega|}{c}\right). \tag{A8b}$$

These equations are valid when $\tilde{r} < |\boldsymbol{\rho} - \mathbf{b}|$.

[1] J. D. Jackson, *Classical Electrodynamics* (Wiley, New York, 1975).
[2] A. Winther and K. Alder, Nucl. Phys. **A319**, 518 (1979).
[3] E. Merzbacher, *Quantum Mechanics*, Sec. 14.6 (Wiley, New York, 1998).
[4] C. A. Bertulani and G. Baur, Phys. Rep. **163**, 299 (1988).
[5] H. Emling, Prog. Part. Nucl. Phys. **33**, 729 (1994).
[6] Ph. Chomaz and N. Frascaria, Phys. Rep. **252**, 275 (1995).
[7] C. A. Bertulani, L. F. Canto, M. S. Hussein, and A. F. R. de Toledo Piza, Phys. Rev. C **53**, 334 (1996).
[8] E. G. Lanza, M. V. Andres, F. Catara, Ph. Chomaz, and C. Volpe, Nucl. Phys. **A613**, 445 (1997).
[9] T. Aumann, P. F. Bortignon, and H. Emling, Annu. Rev. Nucl. Part. Sci. **48**, 351 (1998).
[10] C. A. Bertulani and V. Yu. Ponomarev, Phys. Rep. **321**, 139 (1999).
[11] B. F. Bayman and F. Zardi, Phys. Rev. C **68**, 014905 (2003).
[12] A. J. Baltz, M. J. Rhoades-Brown, and J. Weneser, Phys. Rev. A **44**, 5569 (1991).
[13] K. Rumrich and W. Greiner, Phys. Lett. **A149**, 17 (1990).
[14] D. H. Kobe and P. K. Kennedy, J. Phys. B **16**, L443 (1983).
[15] D. M. Brink, Nucl. Phys. **4**, 215 (1957).